Strain effects on magnetic compensation and spin reorientation transition of Co/Gd synthetic ferrimagnets

Giovanni Masciocchi,[1, 2, a)] Thomas J. Kools,[3] Pingzhi Li,[3] Adrien A. D. Petrillo,[3] Bert Koopmans,[3] Reinoud Lavrijsen,[3] Andreas Kehlberger,[2] and Mathias Kläui[1]

[1)]*Institute of Physics, Johannes Gutenberg University Mainz, Staudingerweg 7, 55128 Mainz, Germany*

[2)]*Sensitec GmbH, Walter-Hallstein-Straße 24, 55130 Mainz, Germany*

[3)]*Department of Applied Physics, Eindhoven University of Technology, P. O. Box 513, 5600 MB Eindhoven, The Netherlands*

(Dated: 2 June 2023)

Synthetic ferrimagnets are an attractive materials class for spintronics as they provide access to all-optical switching of magnetization and, at the same time, allow for ultrafast domain wall motion at angular momentum compensation. In this work, we systematically study the effects of strain on the perpendicular magnetic anisotropy and magnetization compensation of Co/Gd and Co/Gd/Co/Gd synthetic ferrimagnets. Firstly, the spin reorientation transition of a bilayer system is investigated in wedge type samples, where we report an increase in the perpendicular magnetic anisotropy in the presence of in-plane strain. Using a model for magnetostatics and spin reorientation transition in this type of system, we confirm that the observed changes in anisotropy field are mainly due to the Co magnetoelastic anisotropy. Secondly, the magnetization compensation of a quadlayer is studied. We find that magnetization compensation of this synthetic ferrimagnetic system is not altered by external strain. This confirms the resilience of this material system against strain that may be induced during the integration process, making Co/Gd ferrimagnets suitable candidates for spintronics applications.

I. INTRODUCTION

Recent advances in spintronics have opened new possibilities for electronic applications beyond the CMOS standard. New concepts of high density and ultrafast non-volatile data storage have been proposed in magnetic memories[1,2]. Throughout the years, magnetic memories have evolved[3,4] exploiting different geometries[5] and new material platforms such as ferrimagnets[6] have been used to improve storage density[7], reading and writing speed[8] and energy efficiency[9,10]. At the same time, single-pulse optical-switching (AOS) of magnetization has reduced the switching speed of the magnetization below ps timescale[11–14]. This bears promise for a new generation of ultrafast data buffering, in a single chip that integrates photonics with spintronics[15–19].

Ferrimagnets are a class of magnets with unbalanced antiparallel-aligned sublattice moments. The compensation of the two inequivalent sublattices, combines the advantages of both antiferromagnets (antiparallel alignment of magnetic moments) and ferromagnets (finite Zeeman coupling and spin polarization)[16,20]. Moreover, the drastic contrast between the two sublattices in non-adiabatic dynamics, could potentially accommodate AOS by a femtosecond laser pulse[12,16]. Single-pulse AOS is typically observed in rare earth–transition metal (RE–TM) ferrimagnetic alloys like GdFeCo[20] or in multilayer synthetic ferrimagnet, such as Co/Gd and $[Co/Tb]_n$[21,22]. In particular, the one based on multilayer of Co/Gd is a good candidate for integrated opto-spintronics devices as it shows AOS - without the constrains on the composition as imposed by alloy system[23,24] - and at the same time exhibits magnetic and angular momentum compensation, allowing ultrafast domain wall motion[25,26]. For instance, the integration of Co/Gd synthetic ferrimagnets in an optically switchable magnetic tunnel junction has been recently reported[27].

When it comes to technological implementation, strain induced effects must be considered, which could be incurred from processing steps such as packaging and layer deposition[28]. Intrinsic stresses and strain could affect the magnetic anisotropy via changes to the spin-orbit coupling (SOC)[29] or to the magnetization compensation of ferrimagnets especially in RE–TM alloys[30,31] where compensation temperature has been reported to be affected by strain[32,33]. However, in spite of being omnipresent in applications[34–36], the effect of strain are not commonly studied in synthetic ferrimagnets. In this work, we present a systematic study of the effects of strain on Co/Gd synthetic ferrimagnets. By the application of external strain, using substrate bending, we investigate the impact of strain on the perpendicular magnetic anisotropy (PMA) and the magnetization compensation of [Co/Gd] and $[Co/Gd]_2$ multilayers, respectively. Using wedge samples in a bilayer system of Co/Gd and polar magneto-optic Kerr effect (pMOKE) measurements, we confirm that the PMA is increased by in-plane tensile strain and a negative magnetostriction is reported. By including the contribution of the strain-anisotropy for this system in a model for the magnetostatics, we show that the effects of strain on the magnetization are mainly due to the modification of the spin-orbit coupling within the magnetic layer and at the the Pt/Co interface that increases the magnetic anisotropy via magnetoelastic coupling. Additionally, we find that the magnetization compensation point is not affected significantly by strain, as the magnetoelastic coupling affects the anisotropy rather than the magnetization of the two sublattices. Our study explores the mechanisms that underlie the influence of strain on the magnetic anisotropy of Co/Gd ferrimagnets and contributes to a better understanding of the magnetoelastic effects of fer-

[a)]Electronic mail: gmascioc@uni-mainz.de

rimagnetic multilayers. These results could be employed for the optimization and development of spintronics devices, as well as for potential applications in fields such as magnetic memory and sensing.

II. METHODS AND SAMPLE FABRICATION

The samples were grown on a 1.5 μm thick, thermally oxidized SiOx on top of a 625 μm thick Si substrate by DC magnetron sputtering in a chamber with a typical base pressure of 5×10^{-9} mBar. To obtain a variable thickness (wedge) along the sample surface, a shutter in the close proximity of the sample is gradually closed during deposition. This allows to study the compensation and spin reorientation transition (SRT) within a single sample. Two types of samples are realized. Firstly, a bilayer of Ta(4 nm)/Pt(4)/ Co(0-2)/Gd(t_{Gd})/TaN(4) with a constant Gd layer on top of a Co wedge is considered to study the SRT. In addition, a quadlayer of Ta(4)/Pt(4)/Co(0.6)/Gd(0-2)/Co(0.6)/Gd(1.5)/TaN(4), this time with a Gd wedge, is grown to study the magnetization compensation.

The magnetic properties of these wedge samples were investigated by pMOKE with a 658 nm laser. In this configuration, we mostly probe the out-of-plane (OOP) component of the Co magnetization[37] as we measure positive remanence in Co dominated samples and negative remanence for Gd dominated samples. According to Fig. 1 (a), the surface of the sample is scanned along the y-direction using a focused laser spot with a spot-size of $\simeq$250 μm diameter. Accordingly, the local magnetic properties and hysteresis loops can be measured as a function of layer thickness, with a negligible thickness gradient < 0.025 nm within the used laser spot. All the measurements are performed at room temperature. To apply in-plane tensile strain to our multilayer, the substrate is mechanically bent using a three-point method[38]. A square sample of 1 by 1 cm is vertically constrained on two sides and pushed uniformly from below by a cylinder that has off-centered rotation axis. The device generates a tensile strain in the plane of the sample when the cylinder is rotated. As previously reported, the tensile strain is uniaxial along x and uniform in the measured area of the sample. The in-plane strain magnitude is 0.1% and has been measured with a strain gauge (RS PRO). More details about the strain generating device can be found in section S1 of the supplementary information.

III. RESULTS AND DISCUSSION

A. Spin reorientation transition in Co/Gd bilayer

The use of magnetic materials for high density data storage requires magnetic systems that are OOP magnetized[39,40]. In thin films, an OOP magnetic easy axis can be obtained by magnetocrystalline anisotropy induced at the interface with heavy metal[41,42]. In addition to that, strain has been shown to affect the magnetic easy axis direction in systems with PMA[43]. To understand the effect of external strain on Co/Gd systems with PMA, we investigate bilayer samples consisting of Ta(4 nm)/Pt(4)/ Co(0-2)/Gd(t_{Gd})/TaN(4). Specifically, the Co thickness is varied between 0 and 2 nm over a few mm along the y direction, whereas t_{Gd} is constant (as in Fig. 1 (a)). In this system, the balance between the interfacial anisotropy energy (magnetocrystalline anisotropy energy at the Pt/Co interface) and demagnetization energy determines the effective magnetic anisotropy. In such system, the demagnetization energy increases with the thickness of the Co magnetic layer, and consequently, the magnetization will go from out-of-plane (OOP) to in-plane (IP). To probe the magnetization of our wedge sample, we record hysteresis loops from the pMOKE signal. We repeat the measurement moving the laser spot along the wedge in the y direction. Firstly, a sample where t_{Gd}=0 is considered. This measurement can be seen in Figs. 1 (b) and (c). Fig. 1 (b) reports the magnetic response of the Ta(4 nm)/Pt(4)/Co(0-2)/TaN(4) sample to an OOP magnetic film for different t_{Co}. The effective anisotropy K_{eff} was estimated[41] recording hysteresis loops with magnetic field applied OOP and IP and the corresponding anisotropy energy per unit area is $K_s = 1.7$ mJ/m^2. For $t_{Co} = 1.35$ nm the square-shaped loop indicates PMA with K_{eff}= 1.5(2)$\times 10^5$ J/m^3. A value of $M_{Co} = 1.3$ MA/m was used in the calculation. As the thickness of Co is increased (moving the laser spot along the wedge direction - y) the remanence and squareness of the hysteresis loop decreases together with the PMA of the system. For $t_{Co} = 2.00$ nm, the sample is IP magnetized and K_{eff} = -0.8(2)$\times 10^5$ J/m^3 is negative. The OOP to IP transition occurs at $t_{Co} = 1.85(2)$ nm in this system.

To investigate the effects of externally applied in-plane strain, we repeat the measurement while the sample is mechanically bent. The magnetization is coupled to the external strain and can be described by the expression for the anisotropy energy[38]:

$$K_{ME} = -\frac{3}{2}\lambda_s Y \varepsilon, \tag{1}$$

where λ_s is the saturation magnetostriction, Y is the Young's modulus and ε is the strain. If the strain in the film is non-zero, the magneto-elastic coupling of Co contributes in principle to the effective anisotropy. Accordingly, the total anisotropy K_{eff} of the magnetic stack is expected to change in the presence of external strain. Fig. 1 (c) shows the OOP hysteresis loops of Ta(4 nm)/Pt(4)/Co(1.85)/TaN(4) sample before (blue) and after (red) the application of $\varepsilon_{xx} = 0.1\%$. We observe that the magnetization curves are changed in the presence of in-plane strain. The area enclosed between the two curves below saturation can be calculated and is used to determine the magnetoelastic anisotropy K_{ME}[44]. In this system, the strain-induced magnetoelastic anisotropy $K_{ME} = 0.02\ mJ/m^2$ is positive, as we expect from a material with negative magnetostriction like Co[43,45]. More details about the calculations of magnetoelastic anisotropy can be found in section S1 of the supplementary information. Accordingly, the PMA is increased by the applied strain, i.e. the system is expected to be OOP magnetized for thicker Co if compared to samples without strain.

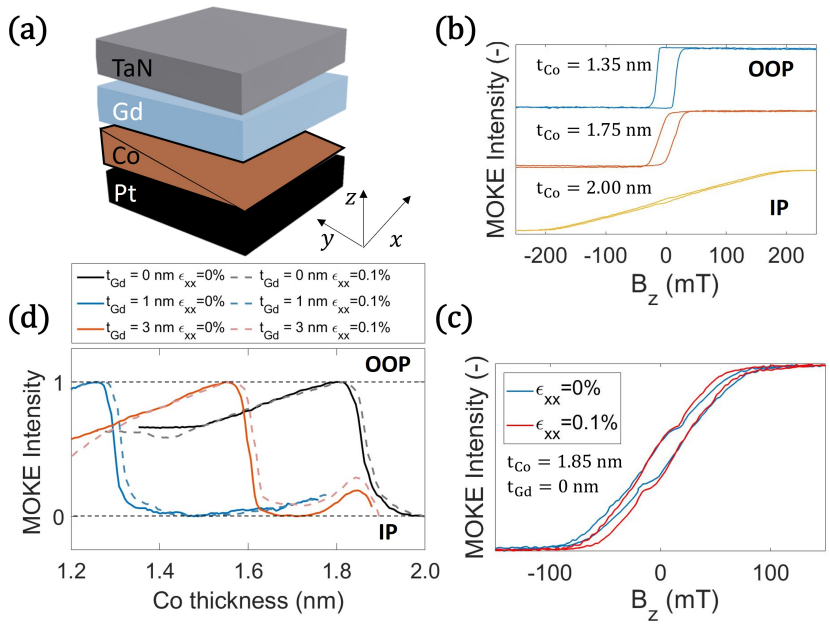

FIG. 1: (a) Sample sketch of the Co/Gd synthetic ferrimagnet used for the spin reorientation transition studies. The red arrow indicates the direction of the applied tensile strain. (b) hysteresis loops of a Pt/Co/TaN stack for different Co thicknesses, the magnetic field was in the OOP direction, along z. (c) OOP hysteresis loops of Pt/Co(1.85 nm)/TaN before (blue) and after (red) application of 0.1% in-plane strain. (d) MOKE intensity scan at remanence (no applied magnetic field) of Pt/Co/Gd/TaN films along the Co wedge before (solid lines) and during (dashed lines) the application of in-plane strain. Three different thicknesses of the Gd layer t_{Gd}=0, 1 and 3 nm have been considered and are reported, in order, in black, blue and orange.

After this preliminary study on Pt/Co systems, we focused our attention on the magnetostriction of Co/Gd multilayers. In Co-Gd alloys the magnetostriction has been reported to be strongly dependent on the composition[29,46] due to the structural modification occurring with different atomic content. In contrast to this case, the effects of magnetostriction of a multilayer, are expected to be dependent on the magnetoelastic coupling of the individual layers[47].

To study the magnetostriction of a Co/Gd multilayer, a constant layer of Gd on top of the Co wedge is added. To perform thickness dependent studies, a thickness $t_{Gd} = 1$ nm and 3 nm is considered. In the bilayer system, the magnetization in the Gd layers is mainly induced at the interface with the Co layer, and couples anti-parallel the Co magnetization[21]. Accordingly, t_{Co} required to reach SRT is expected to change with increasing t_{Gd}[48]. To compare the SRT of Ta(4 nm)/Pt(4)/Co(0-2)/Gd(t_{Gd})/TaN(4) samples with different t_{Gd} we performed remanent intensity scan along our Co wedge, in addition to hysteresis loop measurements. After the sample is saturated with an OOP magnetic field of 1T, we determine the thickness-dependent remanence from the pMOKE signal without external magnetic field. The remanent intensity scans are reported in Fig. 1 (d). As the pMOKE signal is mainly sensitive to the OOP component of Co magnetization, the normalized remanent intensity will drop to zero at the SRT, when the magnetization rotates IP. The SRT can be observed in Fig. 1 (d) in samples with different thicknesses of Gd before and after the application of strain. As previously reported[48] the critical thickness $t_{Co} = t_c$ at which SRT occurs, changes significantly in the presence of a Gd layer. For all the considered samples, the in-plane strain shifts the OOP to IP transition towards larger Co thickness. This suggests that the effective magnetostriction of the Co/Gd bilayer is negative and its value $\lambda_s = -10(5) \times 10^{-6}$ is not significantly altered by the presence of the Gd layer.

To obtain a quantitative understanding of the shape of the spin reorientation boundary, we employ an analytical model[48] describing the magnetostatic free energy of the anisotropy, which is zero at the SRT boundary. The first constituent energies of the model are the demagnetization energies of the Co layer

$$E_{d,Co} = \frac{1}{2}\mu_0 \int_0^y M_{Co}^2\, dq = \frac{1}{2}\mu_0 M_{Co}^2 y \tag{2}$$

and of the Gd layer

$$E_{d,Gd} = \frac{1}{2}\mu_0 \int_0^x M_{Gd}^2 exp(-2q/\lambda_{Gd})\, dq = \frac{1}{4}\mu_0 M_{Gd}^2 \lambda_{Gd}\left(1 - \exp\left(\frac{-2x}{\lambda_{Gd}}\right)\right) \tag{3}$$

where λ_{Gd} is the characteristic decay length of the Gd magnetization, which is induced at the Co/Gd interface, M_{Co} is the magnetization of the Co layer, M_{Gd} is the effective Gd magnetization at the interface between Co and Gd and x and y are, respectively, the Gd and Co thicknesses in the diagram of Fig.2 (a). The plot axes in Fig.2 (a) have been inverted for a better comparison with the other figures. The magnetocrystalline anisotropy is included with the term

$$E_K = K_s - \Delta K\left(1 - \exp\left(\frac{-2x}{\lambda_K}\right)\right), \tag{4}$$

and it is also considered to decay with a characteristic decay length λ_K and magnitude ΔK. The second term in Eq. 4 phenomenologically addressed the experimentally observed decay in the effective anisotropy, which may be caused by sputter induced disordering of the Co[49]. Using a numerical fit to the experimentally determined SRT, the parameters λ_K, λ_{Gd} and ΔK for our Co/Gd bilayer are determined. All the other parameters were either experimentally measured or taken from literature and are reported in Table S.1 , section S2 of the supplementary information. In addition to the anisotropy term, an additional energy term E_{mix} is included in the model. E_{mix} takes into account the mixing at the magnetic layer interfaces where the local net magnetization is zero. More details about the expression for this term and the determination of the fitting parameters can be found in the supplementary information and in the work of Kools et al.[48]. In this model, the expression of the total free energy density per unit area is, considering all the terms mentioned so far:

$$E_{tot} = -E_K - E_{mix} + E_{d,Co} + E_{d,Gd}. \tag{5}$$

The magnetocrystalline anisotropy energy per unit area K_s, due to the Pt/Co interface is assumed constant.

Eq. 5, describing the total energy of a Ta(4nm)/Pt(4)/Co(t_{Co})/Gd(t_{Gd})/TaN(4) sample, can be solved for y (t_{Co}) by imposing $E_{tot} = 0$ (spin reorientation transition). The solution for the SRT obtained with the model described above is reported in Fig. 2 (a) with a blue solid line in a phase diagram where t_{Gd} (x) and t_{Co} (y) are continuously varied from 0 to 3 nm and from 0 to 2 nm, respectively. Together with the calculations, the SRT measured experimentally without externally applied strain is reported with blue diamonds in Fig. 2 (a). The experimental data, follow well the general trend of the calculations. Discrepancies between model and experimental values for $t_{Gd} = 0$, might be due to additional mixing between the layers.

To include the effects of strain, a magnetoelastic anisotropy K_{ME} is added to Eq. 5 that becomes

$$E_{tot} = -E_K - E_{mix} - K_{ME} + E_{d,Co} + E_{d,Gd}. \tag{6}$$

In our case $K_{ME} = 0.02$ mJ/m^2 corresponds to the value of magnetoelastic anisotropy induced with 0.1% externally applied in-plane strain in our experiments. As showed in Fig. 1 (d), we do not observe significant changes to K_{ME} with increasing t_{Gd}. Again considering the SRT-boundary to be at $E_{tot} = 0$, the solution of Eq. 6 (that includes the magnetoelastic term) is reported in Fig. 2 (a) with an orange solid line. As expected from a material with negative magnetostriction, K_{ME} sums to K_s and the PMA is enhanced by in-plane strain. The SRT calculated including K_{ME} to Eq. 6 is consequently shifted to larger values of t_{Co}. This trend is in agreement with

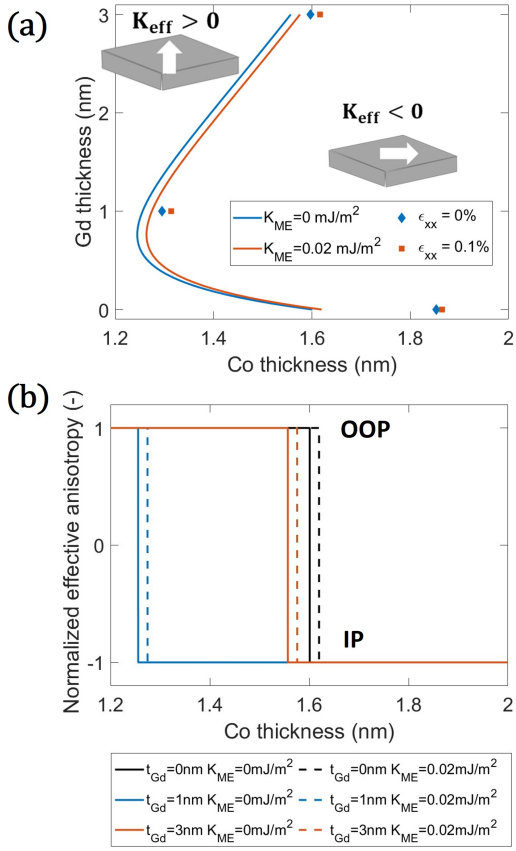

FIG. 2: (a) 2D phase diagram of the SRT of the a Ta(4nm)/Pt(4)/Co(t_{Co})/Gd(t_{Gd})/TaN(4) stack as a function of t_{Gd} (x) and t_{Co} (y). The axes have been inverted for a better comparison with other figures. Blue diamonds and red squares correspond to the experimental data, reported without and with strain applied, respectively. The solid lines indicate the calculated values using the model for the magnetostatics and Eq. 6. A magnetoelastic anisotropy $K_{ME} = 0$ and 0.02 mJ/m^2 is considered, respectively, for the blue and orange curve. (b) Spin reorientation transition of a Ta(4)/Pt(4)/Co(t_{Co})/Gd(t_{Gd})/TaN(4) sample calculated for values of t_{Gd}=0, 1 and 3 nm and plotted as a function of t_{Co}. The SRT is represented here by a step function. Solid and dashed lines consider $K_{ME} = 0$ and 0.02 mJ/m^2, respectively.

the experimentally determined SRT when and external strain $\varepsilon_{xx} = 0.1\%$ is applied (orange squares in Fig.2 (a)).

Another way to visualize the SRT is solving Eq. 6 for fixed values of t_{Gd} and obtaining the critical thickness of t_{Co} such that $E_{tot} = 0$. Then, the SRT can be represented as a step function in the diagram of Fig. 2 (b), analogue to the MOKE remanence scan shown in Fig. 1 (d). The values of Gd thicknesses considered are $t_{Gd} = 0$, 1 and 3 nm and are plotted in Fig. 2 (b) with solid lines in black, blue and orange, in order. Solid lines consider $K_{ME} = 0$ mJ/m^2. Dashed lines consider instead $K_{ME} = 0.02$ mJ/m^2 in Fig. 2 (b). The information contained here can be correlated to the experimental remanent intensity scan in Fig. 1 (d). Comparing Fig. 2 (b) with Fig. 1 (d), a similar behavior can be observed. Firstly we can note that the model predicts the SRT to shift when the thickness of the Gd layer is $t_{Gd} > 0$. Secondly, we observe a similar shift of the SRT point in Fig. 2 (b) and Fig. 1 (d) due to the

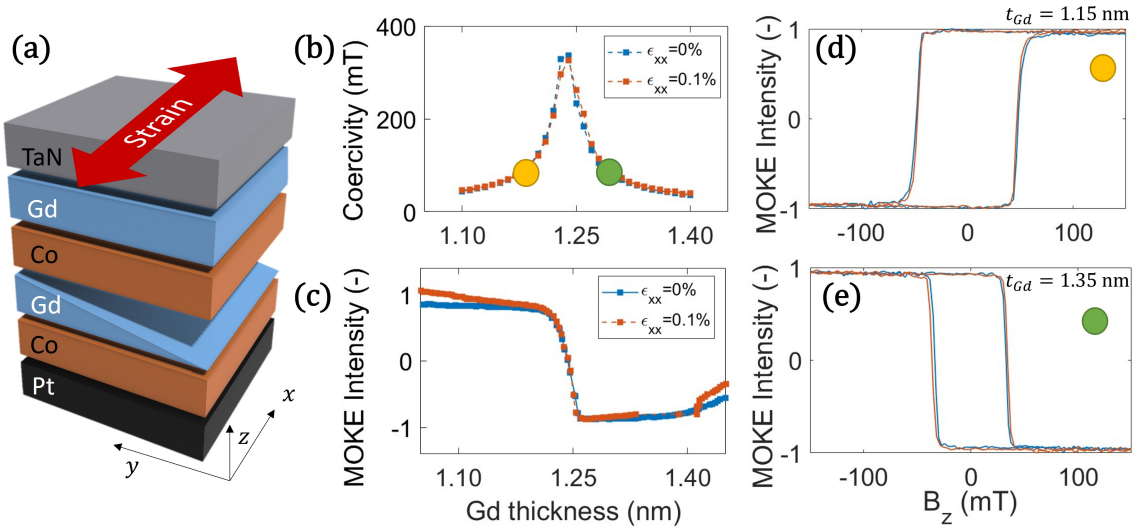

FIG. 3: (a) Layerstack consisting of a Co/Gd quadlayer used to obtain magnetization compensation. In this case, the bottom Gd layer is varied along the sample surface while all the other layers thickness is kept constant. (b) Coercivity and (c) remanent pMOKE intensity scan as a function of t_{Gd}. Measurements before (blue) and after (orange) application of in-plane strain are reported. (d) Hysteresis loops in the Co dominated and (e) Gd dominated state. Both curves with (orange) and without (blue) in-plane strain applied are shown. The magnetic field was applied in the OOP direction, along z.

effect of magnetoelastic anisotropy and of the external strain, respectively. As we expect from a material with negative magnetostriction, K_s adds to K_{ME}, therefore the PMA is increased and the Co/Gd bilayer stays OOP magnetized for thicker Co (corresponding to larger $E_{d,Co}$). We confirm that the major effect of strain on the Ta(4 nm)/Pt(4)/ Co(0-2)/Gd(t_{Gd})/TaN(4) sample is the alteration of the PMA. Moreover, the estimated effective magnetostriction of the stack - $\lambda_s = -10(5) \times 10^{-6}$ - is not significantly altered by the presence of the Gd layer in the thickness range considered.

In this section, we examined the impact of in-plane strain on the effective PMA of a Co/Gd ferrimagnetic bilayer. Our results suggest negative magnetostriction of the stack for the investigated thickness values. We employ a recent model for the magnetostatics of these type of systems, where we include the effects of strain purely as magnetoelastic anisotropy. Our experimental findings are in good agreement with the predictions made by this model, providing deeper understanding of the response of this material platform to external strain.

B. Magnetization compensation in quadlayer systems

In ferrimagnets, magnetization compensation can be achieved. This occurs when the net magnetization $\vec{M}_{tot} = \vec{M}_{Gd} + \vec{M}_{Co}$ vanishes because the magnetization, coming from the two sub-lattices, is equal in magnitude and opposite in sign.

In recent studies, changes to the saturation magnetization in the presence of strain were reported in epitaxial films[31] and rare earth free ferrimagnets[30]. To study the effects of strain on magnetization compensation of synthetic ferrimagnets, we consider a quadlayer sample[48] consisting of Ta(4 nm)/Pt(4)/Co(0.6)/Gd(0-2)/Co(0.6)/Gd(1.5)/TaN(4) as schematically drawn in Fig. 3 (a). In this case, the thickness of the bottom Gd layer is varied between 0 and 2 nm over a few mm, whereas all the other layers have constant thickness. The reason for this choice is that compared to the Co/Gd bilayer, the magnetic volume of the Co is doubled while the number of Co/Gd interfaces where magnetization is induced in the Gd through direct exchange with the Co, is tripled. In this way magnetization compensation can be more readily achieved.

The growing thickness of Gd, increases the contribution of $\vec{M}_{Gd}$ to $\vec{M}_{tot}$. For this reason, some areas of the wedge sample will be Co-dominated (for $t_{Gd} < t_{comp}$) and other will be Gd-dominated (for $t_{Gd} > t_{comp}$) with $\vec{M}_{tot} = 0$ at $t_{Gd} = t_{comp}$. Here, t_{comp} is the thickness where magnetization compensation is obtained. At magnetization compensation two effects are expected: a divergence of the coercivity and a sign change in the remanent pMOKE signal (Kerr rotation, normalized to its value in absence of Gd). The measurements for coercivity and intensity are reported in Figs. 3 (b) and (c), respectively. The coercivity data were extracted from hysteresis loops measured across the wedge direction (along y). The reason for the sign change in the pMOKE signal, is the alignment of the Gd magnetization along the field direction, in the Gd dominated regime. We report magnetization compensation in this quad-layer for $t_{Gd} = 1.25$ nm.

In a similar fashion to what we have done investigating the PMA in the bilayer system, we repeat the experiment in the presence of ε_{xx} =0.1% in-plane strain. The results are reported in orange in Figs. 3 (b) and (c). Remarkably, the compensation point of the Co/Gd quadlayer is unchanged by the application of this externally applied strain.

Figs. 3 (d) and (e) contain OOP hysteresis loops of Ta(4 nm)/Pt(4)/Co(0.6)/Gd(t_{Gd})/Co(0.6)/Gd(1.5)/TaN(4) samples for $t_{Gd} = 1.15$ nm and $t_{Gd} = 1.35$ nm, respectively, and further show the effects of magnetization compensation. The sample is in this case OOP magnetized. As the thickness of Gd is increased, the magnetization of the sample goes from

Co dominated (Fig. 3 (d)) to Gd dominated (Fig. 3 (e)). The inversion of hysteresis loops happens because for $t_{Gd} > 1.25$ *nm* the Co-magnetization aligns antiparallel to the field, leading to the change in sign of the pMOKE signal. When the measurement is repeated in the presence of $\varepsilon_{xx} = 0.1\%$ strain (orange line), no significant changes to the remanent intensity or coercivity are reported, if compared to the unstrained case (blue line). This suggests that magnetization compensation can be achieved in these multilayer systems in the presence of external strain and, most importantly, that the magnetization compensation point is unaffected, in contrast with what has been recently observed in ferrimagnetic alloys[32,33].

In the related work of Wang and coworkers[33] strain is observed to induce changes to the compensation temperature of GdFeCo ferrimagnetic alloys and those changes in compensation are attributed to lattice constant variation with strain. As explained by first principle calculations, this lattice strain alters the exchange coupling strength in GdFeCo and the moment of the Gd accordingly. This might be different in the case of synthetic ferrimagnets.

Synthetic ferrimagnets have the two sublattices confined in separate layers and the Gd magnetization is induced at the Co/Gd interface where the exchange energy is maximum[21,23]. In synthetic ferrimagnets, magnetization compensation is due to the balance in Co magnetization and the Gd magnetization[25,48] in the individual layers and the total magnetic moment per unit area $\vec{M}_{tot}$ is obtained by integrating the magnetization of the Co and Gd sublattices over the respective layer thicknesses.

In multilayer samples with PMA, the dominant effect of in-plane strain in the order of 0.1% is the alteration of the spin orbit coupling within one layer[50]. This alters the magnetocrystalline anisotropy energy of the system[51] rather than the magnetic moment of Co and Gd within one layer. Accordingly, in a ferrimagnetic multilayer in-plane strain is not expected to affect the induced magnetic moment from the Co onto the Gd, thus not altering magnetization compensation. This is consistent with our observations of a strain-independent magnetization compensation in a synthetic ferrimagnet for the magnitudes of strain considered.

IV. CONCLUSIONS

This work reveals the effect that external strain has on PMA and magnetization compensation of Co/Gd systems at room temperature. Growing wedge samples, where the thickness of one of the magnetic layers was varied, has allowed us to determine thickness dependent transition in the magnetostatics of this multilayer system. Deliberate in-plane strain was applied to the sample. In a bilayer Pt/Co/Gd system, we experimentally show that a sizable magnetoelastic coupling changes the SRT in the presence of strain. The contribution of the strain-anisotropy for this system has been included in a model for the magnetostatics, describing the experimental observations well if an effective negative magnetostriction is considered. In a Pt/Co/Gd/Co/Gd quadlayer we obtain magnetization compensation of the two sub-lattices by varying the thickness of the bottom Gd layer. Here, we find that the application of in-plane strain does not affect the magnetization compensation. The induced magnetic moment from the Co onto the Gd, being an interface effect in a multilayer system, is not altered by such mechanical deformation. To conclude, this work provides a broad understanding of the magnetoelastic properties of these multilayer systems. As PMA and magnetic compensation are maintained in the presence of externally applied strain, this material system is a good candidate for technological implementation of ferrimagnets.

SUPPLEMENTARY MATERIAL

See supplementary material for magnetostatics model for the spin reorientation transition and for more details about the setup used for application of strain.

ACKNOWLEDGMENTS

This project has received funding from the European Union's Horizon 2020 research and innovation program under the Marie Skłodowska-Curie grant agreement No 860060 "Magnetism and the effect of Electric Field" (MagnEFi), the Deutsche Forschungsgemeinschaft (DFG, German Research Foundation) - TRR 173 - 268565370 (project A01 and B02) and the Austrian Research Promotion Agency (FFG). The authors acknowledge support by the Max-Planck Graduate Centre with Johannes Gutenberg University.

AUTHOR DECLARATIONS

Conflict of interest

The authors have no conflicts to disclose.

DATA SHARING POLICY

The data that support the findings of this study are available from the corresponding author upon reasonable reques.

[1]T. Endoh, H. Honjo, K. Nishioka, and S. Ikeda, "Recent progresses in STT-MRAM and SOT-MRAM for next generation MRAM," in *2020 IEEE Symposium on VLSI Technology* (IEEE, 2020) pp. 1–2.

[2]S. S. Parkin, M. Hayashi, and L. Thomas, "Magnetic domain-wall racetrack memory," Science **320**, 190–194 (2008).

[3]S. Tehrani, "Status and outlook of MRAM memory technology," in *2006 International Electron Devices Meeting* (IEEE, 2006) pp. 1–4.

[4]K. Garello, F. Yasin, and G. S. Kar, "Spin-orbit torque MRAM for ultrafast embedded memories: From fundamentals to large scale technology integration," in *2019 IEEE 11th International Memory Workshop (IMW)* (IEEE, 2019) pp. 1–4.

[5]K. Gu, Y. Guan, B. K. Hazra, H. Deniz, A. Migliorini, W. Zhang, and S. S. Parkin, "Three-dimensional racetrack memory devices designed from freestanding magnetic heterostructures," Nature Nanotechnology **17**, 1065–1071 (2022).

[6] S.-H. Yang, K.-S. Ryu, and S. Parkin, "Domain-wall velocities of up to 750 m s- 1 driven by exchange-coupling torque in synthetic antiferromagnets," Nature nanotechnology **10**, 221–226 (2015).

[7] R. Tomasello, V. Puliafito, E. Martinez, A. Manchon, M. Ricci, M. Carpentieri, and G. Finocchio, "Performance of synthetic antiferromagnetic racetrack memory: domain wall versus skyrmion," Journal of Physics D: Applied Physics **50**, 325302 (2017).

[8] S.-H. Yang, C. Garg, T. Phung, C. Rettner, and B. Hughes, "Spin-orbit torque driven one-bit magnetic racetrack devices-memory and neuromorphic applications," in *2019 International Symposium on VLSI Technology, Systems and Application (VLSI-TSA)* (IEEE, 2019) pp. 1–2.

[9] Q. Shao, Z. Wang, and J. J. Yang, "Efficient AI with MRAM," Nature Electronics **5**, 67–68 (2022).

[10] S. Parkin and S.-H. Yang, "Memory on the racetrack," Nature nanotechnology **10**, 195–198 (2015).

[11] I. Radu, K. Vahaplar, C. Stamm, T. Kachel, N. Pontius, H. Dürr, T. Ostler, J. Barker, R. Evans, R. Chantrell, *et al.*, "Transient ferromagnetic-like state mediating ultrafast reversal of antiferromagnetically coupled spins," Nature **472**, 205–208 (2011).

[12] T. Ostler, J. Barker, R. Evans, R. Chantrell, U. Atxitia, O. Chubykalo-Fesenko, S. El Moussaoui, L. Le Guyader, E. Mengotti, L. Heyderman, *et al.*, "Ultrafast heating as a sufficient stimulus for magnetization reversal in a ferrimagnet," Nature communications **3**, 1–6 (2012).

[13] A. V. Kimel and M. Li, "Writing magnetic memory with ultrashort light pulses," Nature Reviews Materials **4**, 189–200 (2019).

[14] P. Zhang, T.-F. Chung, Q. Li, S. Wang, Q. Wang, W. L. Huey, S. Yang, J. E. Goldberger, J. Yao, and X. Zhang, "All-optical switching of magnetization in atomically thin CrI_3," Nature materials **21**, 1373–1378 (2022).

[15] E. K. Sobolewska, J. Pelloux-Prayer, H. Becker, G. Li, C. S. Davies, C. Krückel, L. A. Félix, A. Olivier, R. C. Sousa, I.-L. Prejbeanu, *et al.*, "Integration platform for optical switching of magnetic elements," in *Active Photonic Platforms XII*, Vol. 11461 (SPIE, 2020) pp. 54–72.

[16] S. K. Kim, G. S. Beach, K.-J. Lee, T. Ono, T. Rasing, and H. Yang, "Ferrimagnetic spintronics," Nature Materials **21**, 24–34 (2022).

[17] L. Avilés-Félix, L. Álvaro-Gómez, G. Li, C. Davies, A. Olivier, M. Rubio-Roy, S. Auffret, A. Kirilyuk, A. Kimel, T. Rasing, *et al.*, "Integration of Tb/Co multilayers within optically switchable perpendicular magnetic tunnel junctions," Aip Advances **9**, 125328 (2019).

[18] M. L. Lalieu, R. Lavrijsen, and B. Koopmans, "Integrating all-optical switching with spintronics," Nature communications **10**, 110 (2019).

[19] H. Becker, C. J. Krückel, D. Van Thourhout, and M. J. Heck, "Out-of-plane focusing grating couplers for silicon photonics integration with optical MRAM technology," IEEE Journal of Selected Topics in Quantum Electronics **26**, 1–8 (2019).

[20] K.-J. Kim, S. K. Kim, Y. Hirata, S.-H. Oh, T. Tono, D.-H. Kim, T. Okuno, W. S. Ham, S. Kim, G. Go, *et al.*, "Fast domain wall motion in the vicinity of the angular momentum compensation temperature of ferrimagnets," Nature materials **16**, 1187–1192 (2017).

[21] M. Lalieu, M. Peeters, S. Haenen, R. Lavrijsen, and B. Koopmans, "Deterministic all-optical switching of synthetic ferrimagnets using single femtosecond laser pulses," Physical review B **96**, 220411 (2017).

[22] L. Avilés-Félix, A. Olivier, G. Li, C. S. Davies, L. Álvaro-Gómez, M. Rubio-Roy, S. Auffret, A. Kirilyuk, A. Kimel, T. Rasing, *et al.*, "Single-shot all-optical switching of magnetization in Tb/Co multilayer-based electrodes," Scientific reports **10**, 1–8 (2020).

[23] M. Beens, M. L. Lalieu, A. J. Deenen, R. A. Duine, and B. Koopmans, "Comparing all-optical switching in synthetic-ferrimagnetic multilayers and alloys," Physical Review B **100**, 220409 (2019).

[24] Y. Xu, M. Deb, G. Malinowski, M. Hehn, W. Zhao, and S. Mangin, "Ultrafast magnetization manipulation using single femtosecond light and hot-electron pulses," Advanced Materials **29**, 1703474 (2017).

[25] T. H. Pham, J. Vogel, J. Sampaio, M. Vaňatka, J.-C. Rojas-Sánchez, M. Bonfim, D. Chaves, F. Choueikani, P. Ohresser, E. Otero, *et al.*, "Very large domain wall velocities in Pt/Co/GdOx and Pt/Co/Gd trilayers with Dzyaloshinskii-Moriya interaction," EPL (Europhysics Letters) **113**, 67001 (2016).

[26] P. Li, T. J. Kools, B. Koopmans, and R. Lavrijsen, "Ultrafast racetrack based on compensated Co/Gd-based synthetic ferrimagnet with All-Optical Switching," Advanced Electronic Materials **9**, 2200613 (2023).

[27] L. Wang, H. Cheng, P. Li, Y. L. van Hees, Y. Liu, K. Cao, R. Lavrijsen, X. Lin, B. Koopmans, and W. Zhao, "Picosecond optospintronic tunnel junctions," Proceedings of the National Academy of Sciences **119**, e2204732119 (2022).

[28] H. Windischmann, "Intrinsic stress in sputter-deposited thin films," Critical Reviews in Solid State and Material Sciences **17**, 547–596 (1992).

[29] K. Twarowski and H. Lachowicz, "Magnetostriction and anisotropy of amorphous Gd-Co RF sputtered thin films," Journal of Applied Physics **50**, 7722–7724 (1979).

[30] Z. Chen, X. Shi, X. Liu, X. Chen, Z. Zhang, and W. Mi, "Modulating saturation magnetization and topological Hall resistivity of flexible ferrimagnetic Mn4N films by bending strains," Journal of Applied Physics **132**, 233906 (2022).

[31] M. Zheng, P. Guan, and H. Fan, "Mechanically enhanced magnetism in flexible semitransparent CuFe2O4/mica epitaxial heterostructures," Applied Surface Science **584**, 152586 (2022).

[32] S. Ota, P. Van Thach, H. Awano, A. Ando, K. Toyoki, Y. Kotani, T. Nakamura, T. Koyama, and D. Chiba, "Strain-induced modulation of temperature characteristics in ferrimagnetic Tb-Fe films," Scientific reports **11**, 1–7 (2021).

[33] J. Wang, M. Li, C. Li, R. Tang, M. Si, G. Chai, J. Yao, C. Jia, and C. Jiang, "Piezostrain-controlled magnetization compensation temperature in ferrimagnetic GdFeCo alloy films," Physical Review B **107**, 184424 (2023).

[34] A. Tavassolizadeh, K. Rott, T. Meier, E. Quandt, H. Hölscher, G. Reiss, and D. Meyners, "Tunnel magnetoresistance sensors with magnetostrictive electrodes: Strain sensors," Sensors **16**, 1902 (2016).

[35] A. M. Sahadevan, R. K. Tiwari, G. Kalon, C. S. Bhatia, M. Saeys, and H. Yang, "Biaxial strain effect of spin dependent tunneling in MgO magnetic tunnel junctions," Applied Physics Letters **101**, 042407 (2012).

[36] Q. Wang, J. Domann, G. Yu, A. Barra, K. L. Wang, and G. P. Carman, "Strain-mediated spin-orbit-torque switching for magnetic memory," Physical Review Applied **10**, 034052 (2018).

[37] J. Erskine and E. Stern, "Magneto-optic Kerr effects in gadolinium," Physical Review B **8**, 1239 (1973).

[38] G. Masciocchi, M. Fattouhi, A. Kehlberger, L. Lopez-Diaz, M.-A. Syskaki, and M. Kläui, "Strain-controlled domain wall injection into nanowires for sensor applications," Journal of Applied Physics **130**, 183903 (2021).

[39] C. Chappert, A. Fert, and F. N. Van Dau, "The emergence of spin electronics in data storage," Nature materials **6**, 813–823 (2007).

[40] B. Tudu and A. Tiwari, "Recent developments in perpendicular magnetic anisotropy thin films for data storage applications," Vacuum **146**, 329–341 (2017).

[41] M. Johnson, P. Bloemen, F. Den Broeder, and J. De Vries, "Magnetic anisotropy in metallic multilayers," Reports on Progress in Physics **59**, 1409 (1996).

[42] F. Den Broeder, W. Hoving, and P. Bloemen, "Magnetic anisotropy of multilayers," Journal of magnetism and magnetic materials **93**, 562–570 (1991).

[43] K. Kyuno, J.-G. Ha, R. Yamamoto, and S. Asano, "Theoretical study on the strain dependence of the magnetic anisotropy of X/Co (X= Pt, Cu, Ag, and Au) metallic multilayers," Journal of applied physics **79**, 7084–7089 (1996).

[44] R. O'Handley, O.-S. Song, and C. Ballentine, "Determining thin-film magnetoelastic constants," Journal of applied physics **74**, 6302–6307 (1993).

[45] S. Hashimoto, Y. Ochiai, and K. Aso, "Perpendicular magnetic anisotropy and magnetostriction of sputtered Co/Pd and Co/Pt multilayered films," Journal of applied physics **66**, 4909–4916 (1989).

[46] K. Twarowski, H. Lachowicz, M. Gutowski, and H. Szymczak, "On the origin of the perpendicular anisotropy and magnetostriction in amorphous RF sputtered Gd Co films," physica status solidi (a) **63**, 103–108 (1981).

[47] G. Masciocchi, J. W. van der Jagt, M.-A. Syskaki, A. Lamperti, N. Wolff, A. Lotnyk, J. Langer, L. Kienle, G. Jakob, B. Borie, *et al.*, "Control of magnetoelastic coupling in Ni/Fe multilayers using He+ ion irradiation," Applied Physics Letters **121**, 182401 (2022).

[48] T. J. Kools, M. C. van Gurp, B. Koopmans, and R. Lavrijsen, "Magnetostatics of room temperature compensated Co/Gd/Co/Gd-based synthetic ferrimagnets," Applied Physics Letters **121**, 242405 (2022).

[49] G. Bertero, T. Hufnagel, B. Clemens, and R. Sinclair, "TEM analysis of Co-Gd and Co-Gd multilayer structures," Journal of materials research **8**, 771–774 (1993).

[50]B. Zhang, K. M. Krishnan, C. Lee, and R. Farrow, "Magnetic anisotropy and lattice strain in Co/Pt multilayers," Journal of applied physics **73**, 6198–6200 (1993).

[51]D. B. Gopman, C. L. Dennis, P. Chen, Y. L. Iunin, P. Finkel, M. Staruch, and R. D. Shull, "Strain-assisted magnetization reversal in Co/Ni multilayers with perpendicular magnetic anisotropy," Scientific reports **6**, 1–8 (2016).

Supplementary material - Strain effects on magnetic compensation and spin reorientation transition of Co/Gd synthetic ferrimagnets

(Dated: 2 June 2023)

S1 -Application of strain

To obtain information about the magnetoelastic properties of the material, the substrate was bent mechanically with a 3 point bending sample holder, as shown schematically in Fig. S1 (a). A square sample of 1 by 1 cm is vertically constrained on two sides and pushed uniformly from below by a cylinder that has an off-centered rotation axis. The device generates a tensile strain in the plane of the sample up to 0.1 % when the cylinder is rotated by 90°. The strain is mostly uniaxial and has been measured with a strain gauge on the substrate surface.

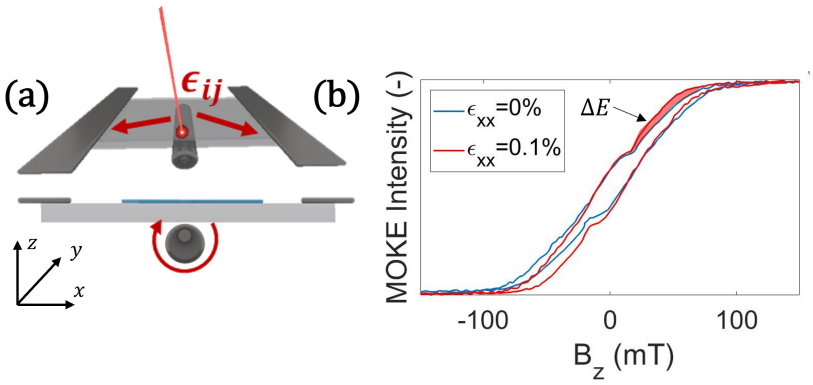

FIG. S 1: (a) schematic of the three point bending method used to externally strain the sample. The strain is mostly uniaxial along the x direction. (b) hysteresis loops measured before (blue) and during (red) application of in-plane strain for a sample of Pt/Co(1.85 nm)/Ta. The area highlighted in red corresponds to the magnetoelastic energy in the strained system. The magnetic field was applied along the OOP direction (z).

Magnetic hysteresis loops are recorded before and after the application of the tensile strain and are used to estimate the magnetoelastic anisotropy. As previously reported[1,2] the magnetic anisotropy K_{eff} is linked to the energy stored in the magnetization curves. For example the PMA energy is given by the area enclosed between the magnetic loops measured with field along IP and OOP direction. If then the strain in the film is non-zero, the magneto-elastic coupling contributes in principle to the effective anisotropy. Two hysteresis loops measurements, before and after the application of strain, are sufficient to estimate K_{ME}. Indeed the total anisotropy of the system is $K_{eff} = K_s$ and $K_{eff} = K_s + K_{ME}$ before and after the application of strain, respectively. The magnetoelastic anisotropy $K_{ME} = -\frac{3}{2}\lambda_s Y \varepsilon$ is linked to reversible part of the hysteresis loops (close to the saturation) according to[3]

$$K_{ME} = M_s \Delta E = -\frac{3}{2}\lambda_s Y \varepsilon \tag{S.1}$$

where ΔE is the anisotropy energy measured by the difference in area enclosed between the strained and unstrained curves below saturation, ε is the strain λ_s is the magnetostriction and Y is the Young's mudulus of the material. In our case $\varepsilon = 0.1\%$ and Y=200 GPa. ΔE corresponds to the reversible part, i.e. the red marked area in Fig. S1 (b). The value of magnetoelastic anisotropy was calculated using the value of saturation magnetization (M_s) of the stack taken from literature and reported in Table S I.

S2 - Magnetostatics model for the Spin Reorientation Transition

In the expression of the free energy, a term describing the effect of intermixing at the multilayer system interfaces is added. The expression is

$$\begin{aligned} &E_{mix} = \tfrac{1}{2}\mu_0 \int_0^{a_0 x} M_{Co}^2 + \left(M_{Gd} exp(-q/\lambda_{Gd})\right)^2 dq = \\ &\tfrac{1}{2}\mu_0 a_0 M_{Co}^2 x + \tfrac{1}{4}\mu_0 \lambda_{Gd} M_{Gd}^2 \left(1 - \exp\left(\tfrac{-2a_0 x}{\lambda_{Gd}}\right)\right). \end{aligned} \tag{S.2}$$

Therefore, the total energy $E_{tot} = -E_K - E_{mix} - K_{ME} + E_{d,Co} + E_{d,Gd}$, including all the terms will be:

$$\begin{aligned} &E_{tot} = -K_s + \Delta K \left(1 - \exp\left(\tfrac{-2x}{\lambda_K}\right)\right) - K_{ME} - \tfrac{1}{2}\mu_0 a_0 M_{Co}^2 x \\ &-\tfrac{1}{4}\mu_0 \lambda_{Gd} M_{Gd}^2 \left(1 - \exp\left(\tfrac{-2a_0 x}{\lambda_{Gd}}\right)\right) + \tfrac{1}{2}\mu_0 M_{Co}^2 y \\ &+\tfrac{1}{4}\mu_0 M_{Gd}^2 \lambda_{Gd} \left(1 - \exp\left(\tfrac{-2x}{\lambda_{Gd}}\right)\right). \end{aligned} \tag{S.3}$$

Here x and y are, respectively, the Gd and Co thicknesses in the phase diagram of Fig. S2. The value of the parameters used in our model are listed in Table S I .

The values of λ_K, λ_{Gd} and Δ_K are instead determined using a numerical fit and are reported in Table S I. To fit this equation to the phase diagram obtained experimentally, it is convenient to find the Co-thickness (y) where the anisotropy energy (E_{tot}) is equal to zero (spin reorientation transition, SRT). Solving Eq. S.3 for y gives:

$$\begin{aligned} &y_0(x) = \tfrac{2}{M_{Co}^2 \mu_0}\left(-\left(K_s - \Delta K\left(1 - \exp\left(\tfrac{-x}{\lambda_K}\right)\right)\right)\right) - \tfrac{1}{2}\mu_0 a_0 M_{Co}^2 x \\ &-\tfrac{1}{4}\mu_0 \lambda_{Gd} M_{Gd}^2 \left(1 - \exp\left(\tfrac{-2a_0 x}{\lambda_{Gd}}\right)\right) + \tfrac{1}{4}\mu_0 M_{Gd}^2 \lambda_{Gd} \left(1 - \exp\left(\tfrac{-2x}{\lambda_{Gd}}\right)\right). \end{aligned} \tag{S.4}$$

Parameter	Value	Description
K_s	1.7 mJ/m^2	Interfacial anisotropy (from exp.)
K_{ME}	0.02 mJ/m^2	Magnetoelastic anisotropy (from exp.)
M_{Co}	1.3 MA/m	Cobalt magnetization (from exp.)
M_{Gd}	1.4 MA/m	Gadolinium magnetization at Co/Gd interface (from Ref.[4])
a_0	0.13 (-)	Growth parameter of intermixing region (from exp.)
λ_K	0.51(15) nm	Change of PMA energy characteristic decay length (Fit parameter)
λ_{Gd}	0.59(22) nm	Gd magnetization decay characteristic decay length (Fit parameter)
Δ_K	$3.96(41)\times10^{-4}$ J/m^2	Change of PMA energy (Fit parameter)

TABLE S I: Parameters used in the model for the magnetostatics of uncompensated Co/Gd synthetic ferrimagnets used for the calculations of the SRT. The term K_{ME} is considered zero for when external strain is not applied to the sample.

Note that for determining the fit parameters, the measurements were taken without externally applied strain. Accordingly, the magnetoelastic energy term K_{ME} is set to zero in Eq. S.4. The experimental data used for the numerical fit are reported in Fig. S2. The sample used for the numerical fit, explores a wide thickness range (Gd from 0 to 6 nm) in a double wedge fashion to improve accuracy. Consequently, the dimensions of this sample exceed the 1x1 cm size of the bending device. For this reason, single wedge samples have been deposited for the strain-dependent study. This means that, on top of the Co wedge, a Gd layer with a constant thickness has been sputtered. Three independent samples have been prepared and studied with Gd thickness t_{Gd} = 0, 1 and 3 nm, in order and are reported in Fig. 1 (d) and Fig. 2 (a) of the main text.

The feature around t_{Gd}=2 nm in Fig. S2 is not captured by out toy model, and might be due to the additional intermixing caused during sputtering, not included in Eq. S.3.

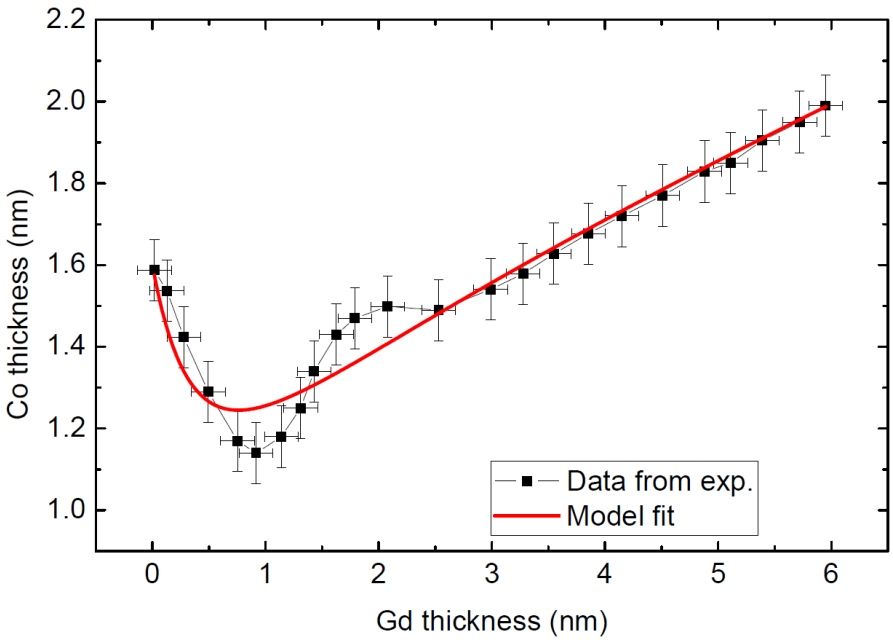

FIG. S 2: Values for the SRT obtained experimentally on a $Ta(4nm)/Pt(4)/\ Co(t_{Co})/Gd(t_{Gd})/TaN(4)$ sample and used to extract the fitting parameters in Eq. S.4.

REFERENCES

[1]Johnson, M. T., Bloemen, P. J. H., Den Broeder, F. J. A., and De Vries, J. J. (1996). Magnetic anisotropy in metallic multilayers. Reports on Progress in Physics, 59(11), 1409.

[2]Baril, L., Gurney, B., Wilhoit, D., Speriosu, V. (1999). Magnetostriction in spin valves. Journal of Applied Physics, 85(8), 5139-5141.

[3]O'Handley, R. C., Song, O. S., Ballentine, C. A. (1993). Determining thin-film magnetoelastic constants. Journal of applied physics, 74(10), 6302-6307.

[4]Kools, T. J., van Gurp, M. C., Koopmans, B., and Lavrijsen, R. (2022). Magnetostatics of room temperature compensated Co/Gd/Co/Gd-based synthetic ferrimagnets. Applied Physics Letters, 121(24), 242405.